

Article

Embodied Energy in the Production of Guar and Xanthan Biopolymers and Their Cross-Linking Effect in Enhancing the Geotechnical Properties of Cohesive Soil

M. Ashok Kumar ¹, Arif Ali Baig Moghal ^{2,*}, Kopparthi Venkata Vydehi ² and Abdullah Almajed ³

¹ Department of Civil Engineering, CVR College of Engineering, Hyderabad 501510, Telangana, India; m.ashokkumar@cvr.ac.in

² Department of Civil Engineering, National Institute of Technology Warangal, Warangal 506004, Telangana, India; kvvydehi252@gmail.com

³ Department of Civil Engineering, College of Engineering, King Saud University, Riyadh 11421, Saudi Arabia; alabduallah@ksu.edu.sa

* Correspondence: baig@nitw.ac.in or reach2arif@gmail.com; Tel.: +91-9989677217

Abstract: Traditional soil stabilization techniques, such as cement and lime, are known for their menacing effect on the environment through heavy carbon emissions. Sustainable soil stabilization methods are grabbing attention, and the utilization of biopolymers is surely one among them. Recent studies proved the efficiency of biopolymers in enhancing the geotechnical properties to meet the requirements of the construction industry. The suitability of biopolymer application in different soils is still unexplored, and the carbon footprint analysis (CFA) of biopolymers is crucial in promoting the biopolymers as a promising sustainable soil stabilization method. This study attempts to investigate the out-turn of cross-linked biopolymer on soils exhibiting different plasticity characteristics (Medium & High compressibility) and to determine the Embodied carbon factor (ECF) for the selected biopolymers. Guar (G) and Xanthan (X) biopolymers were cross-linked at different proportions to enhance the geotechnical properties of soils. Atterberg's limits, Compaction characteristics, and Unconfined Compressive Strength were chosen as performance indicators, and their values were analyzed at different combinations of biopolymers before and after cross-linking. The test results have shown that Atterberg's limits of the soils increased with the addition of biopolymers, and it is attributed to the formation of hydrogels in the soil matrix. Compaction test results reveal that the Optimum Moisture Content (OMC) of biopolymer-modified soil increased, and Maximum Dry Density (MDD) reduced due to the resistance offered by hydrogel against compaction effort. Soils amended with biopolymers and cured for 14, 28, and 60 days have shown an appreciable improvement in Unconfined Compressive Strength (UCS) results. Microlevel analysis was carried out using SEM (Scanning Electron Microscopy) and FTIR (Fourier-transform infrared spectroscopy) to formulate the mechanism responsible for the alteration in targeted performance indicators due to the cross-linking of biopolymers in the soil. The embodied energy in the production of both Guar and Xanthan biopolymers was calculated, and the obtained ECF values were 0.087 and 1.67, respectively.

Keywords: Atterberg's limits; biopolymer cross-linking; carbon footprint analysis; compaction characteristics; compressive strength; guar; xanthan



Citation: Kumar, M.A.; Moghal, A.A.B.; Vydehi, K.V.; Almajed, A. Embodied Energy in the Production of Guar and Xanthan Biopolymers and Their Cross-Linking Effect in Enhancing the Geotechnical Properties of Cohesive Soil. *Buildings* **2023**, *13*, 2304. <https://doi.org/10.3390/buildings13092304>

Academic Editor: Jan Fort

Received: 10 August 2023

Revised: 6 September 2023

Accepted: 8 September 2023

Published: 10 September 2023



Copyright: © 2023 by the authors. Licensee MDPI, Basel, Switzerland. This article is an open access article distributed under the terms and conditions of the Creative Commons Attribution (CC BY) license (<https://creativecommons.org/licenses/by/4.0/>).

1. Introduction

A rise in urbanization is driving the need for development on difficult soils, necessitating the use of appropriate soil stabilization techniques to enhance the soil properties. While lime and cement have been extensively utilized in the last couple of decades, their abnormal use can harm the environment due to associated excessive carbon emissions [1–3]. Researchers are being urged to identify a sustainable material for soil stabilization because standard soil stabilization methods have a high carbon impact [4]. When soil is combined

with lime and cement, its geotechnical properties will change and turn ecologically inert, further altering the pH of natural groundwater and preventing the emergence of plants and fauna [5]. The embodied energy required to produce cement and lime is also considerable [6]. It is crucial to establish a balance between sustainability objectives and the benefits of soil attributes [7].

It is possible to employ fly ash as a soil stabilizer when combined with the appropriate admixtures, but lime leachability must be carefully considered to ensure long-term viability [8]. The particle size distribution of the soil matrix, cohesiveness, and shearing resistance have all changed because of clayey soil mixed with granite dust [9]. The fine content that naturally existing soils possess has an impact on their structure and, thus, their unsaturated behavior, changing the form of the resulting water-retention characteristic curve (WRCC) [10]. Soil reinforcement is an option to enhance the engineering properties to meet the requirements of a subgrade material [11]. Soils treated with calcium-based derivatives and granite dust resulted in the reduction of the pore volume and in the enhancement of tensile strength [12]. Non-availability of cohesive soils has moved the focus to the enrichment of sandy soils to meet the requirements of liner and subbase [13]. Enhancement in soil qualities, including water retention, pollutant mitigation, and shear strength, has been accomplished using bio-geo-engineering techniques such as EICP and MICP. The efficiency of EICP and MICP depends on the microbes present and is more effective in the stabilization of cohesionless soils [5,14]. Biopolymers are gaining the attention of researchers as their application in the field is simpler and more efficient in soil stabilization. Biopolymer-based soil treatment (BPST) research is a recent trend that is environmentally friendly and sustainable in ground improvement and soil treatment [15,16].

Biopolymers are naturally occurring polysaccharides that have been extensively used as viscosifiers in agriculture and the food industry. G, X, starch, and alginate gum are being used to reduce soil permeability, and X is being used to increase soil shear strength [17]. Biopolymers, when added to the soil, react with pore water and form a hydrogel, which further reacts with the soil particles [18]. The physicochemical properties of biopolymers, namely viscosity, hydrogen bonding, and surface characteristics, have a considerable effect on the soil-biopolymer mix. Biopolymer treatment is very effective in treating well-graded soils when compared to poorly graded soils [19]. Desiccation cracking in medium to high plastic clays was effectively controlled by the usage of G, and X was efficient in enhancing the shear strength and permeability of sand and silty sand [20]. Soils treated with X and G have shown great resistance against erosion and are very efficient for use in slope protection [5,21]. Biopolymer dosage depends on soil nature, and most of the soils have shown a remarkable improvement in their geotechnical properties when the dosage is kept at 1–2%. The shear strength of cohesive soils was improved around 2–4 times and 6–8 times for cohesion-less soils [22]. While treating cohesive soils, MDD values were reduced by 1–2 kN/m³, and OMC values were increased proportionately [23,24]. Soil treated with chitosan has displayed a considerable improvement in compressive strength of 4 MPa with an extended curing period of 90 days. Chitosan at high dosages was used for canal lining and was proven to be effective in holding and retaining water [25,26].

Biopolymers initially interact with pore water in the soil to form a 3D network of hydrogels, which further connect the soil particles and create a stabilizing effect. On drying, these hydrogels are converted from a rubbery to a glassy state and influence the improvement of soil strength [27]. The integrity, chemical activity, and mechanical properties of the hydrogels are reliant on the type of biopolymer used and the time taken by the hydrogel to absorb the water to swell before the dilution. To avoid or delay the dilution of hydrogels, biopolymers are usually cross-linked, where the outer chains of biopolymers react with other polymer chains [28]. This process proved to be effective in enhancing the physical integrity and mechanical properties of the hydrogel. Investigation revealed that cross-linking the biopolymers addresses the shortcomings of each biopolymer when individually used in the stabilization of rammed earth [18]. G and X were previously cross-linked, and it has improved the aversion of mine tailings to wind erosion [29]. G and

X were cross-linked, and they were found to be very effective in the stabilization of fly ash suspensions and retarding spontaneous coal combustion to remediate the groundwater [30]. The available literature recommended that both G and X can be cross-linked without adding any external agent [31].

This research provides the embodied carbon footprint of Guar and Xanthan biopolymers from the production stages, which has not been attempted by earlier researchers. Till now, the literature review available deals with studying the effect of the addition of single-type biopolymers in enhancing the geotechnical properties of soil. In the current study, the effect of the addition of cross-linked biopolymers in enhancing the geotechnical properties of cohesive soil has been investigated.

2. Background

An increasing amount of research shows that G and X biopolymers are widely accepted as sustainable soil additives [31]. Despite these materials being derived from natural resources, the various steps in their manufacturing and the use of certain components (not made from natural sources) result in a large amount of CO₂ emissions being released into the environment. The estimation of a product's total CO₂ emissions from its inception through disposal requires a main database, which is frequently challenging to get. As a result, the focus of the current work is on estimating CO₂ emissions using carbon footprint analysis (CFA) from the production stages of G and X, relying on the database from the previous literature and subjected to boundary conditions. The specifications (or conditions) used at each stage of manufacturing are in line with the best yield of the chosen biopolymers.

Furthermore, recent investigations have shown that biopolymer cross-linking can also be adopted in soil stabilization to enhance the targeted geotechnical properties such as strength, permeability, and durability [32]. However, the application of biopolymers in soil stabilization is still limited as their interaction with soils of different mineralogy is not completely understood.

The main objectives of this research are:

- To investigate the effect of biopolymer inclusion and their cross-linking on the soils exhibiting different plasticity characteristics by choosing Atterberg's limits, compaction characteristics, and unconfined compression strength tests as performance indicators.
- To determine the embodied carbon emissions of the selected biopolymers, namely guar and xanthan gum, from the production stages.

3. Materials and Methods

3.1. Biopolymers

Biopolymers, namely G and X, used in the study were collected from SRL Chemicals, Mumbai, India. The properties of biopolymers are described below.

3.1.1. Guar Gum

G is the powdered endosperm of the seeds of *Cyamopsis tetragonolobus*, which is a leguminous crop [21,33]. It is a non-ionic hydrocolloid polysaccharide composed of galactose and mannose structural units [34].

3.1.2. Xanthan Gum

X is a polysaccharide that results from the enzymatic action of a carbohydrate source, such as glucose. *Xanthomonas campestris* is a bacterium that facilitates the process of producing X gum. This gum can be dissolved in both cold and hot water. The viscosity of the medium will be increased when X is added to it, and the solution will display a non-Newtonian property with high pseudo-plasticity [23]. In recent days, the use of biopolymers has been widely seen in the cosmetics industry, agriculture, the food industry, civil engineering, and the drilling industry.

Guar and Xanthan biopolymers were selected for the investigation as they can be cross-linked naturally without adding any external agents. The addition of an external agent may result in undesirable changes in the geotechnical properties when used in field applications [17]. Biopolymers were mixed at dosages of 1G, 2G, 1X, 2X, and 1G + 1X by the weight of dry soil mass. The optimum dosage of biopolymers was fixed as 2% of the dry soil mass. The properties of both G and X are listed in Table 1.

Table 1. Properties of Guar and Xanthan biopolymers.

S. No.	Property	G	X
1	Color	White to pale yellow	White to off-white
2	Ash (%)	2	13
3	Pyruvic acid	--	1.5
4	Loss on drying (%)	13	15
5	pH (1% aqueous solution)	--	6.0–8.0
6	Viscosity (1% aqueous solution at 25 °C)	--	600 mPa·s

(Source: From the manufacturer, SRL Chemicals Pvt Ltd., Mumbai, India).

3.2. Soils

In this study, the effectiveness of biopolymer cross-linking in stabilizing soil was evaluated by conducting laboratory tests on two soils with varying plasticity characteristics. Soils were collected from two different locations, and their characterization was completed following the applicable code. Soil collected from Ibrahimpatnam, Ranga Reddy district, Telangana, India (17.10° N 78.62° E) with high plasticity index was denoted as S1, and the sample collected from Singarayakonda, Prakasam district, Andhra Pradesh, India (15°14'32.1" N 80°01'59.6" E) with medium plasticity index was denoted as S2. Table 2 shows the geotechnical properties of soil samples used for the investigation.

Table 2. Geotechnical Properties of studied soils S1 and S2.

S. No.	Property	Sample S1	Sample S2
1	Liquid Limit (%)	63.2	48.1
2	Plastic Limit (%)	30.9	25.9
3	Plasticity Index (%)	32.3	22.2
4	Free Swell Index (%)	45	12.5
5	Optimum Moisture Content (OMC) (%)	26	11
6	Maximum Dry Density (MDD) (kN/m ³)	14.41	19.22
7	Unconfined Compression strength (kPa)	92.18	121.6
8	Soil Classification (Unified Soil Classification system)	CH	CM

Note: 'OMC' refers to Optimum Moisture Content; 'MDD' refers to Maximum Dry Density; 'CH' refers to High-Compressible Clay; 'CM' refers to Medium-Compressible Clay as per the Unified Soil Classification System (USCS).

In the laboratory, the mechanical and physical properties of virgin soil were examined. The soil samples S1 and S2 were next treated with independent doses of G and X. Later, each soil was treated with a mixture of G and X to evaluate the variation in the targeted geotechnical parameters. The ideal biopolymer dosage for soil is 2% by dry soil weight, as seen from earlier studies [18,35]. Hence, in the present study, the dosage of independent biopolymer is limited to 2% by the dry weight of soil, and for cross-linking cases, the dosage is limited to 1% (for each biopolymer). Table 3 outlines the various soil and biopolymer combinations that were used in this study.

Table 3. Different combinations of soils and biopolymer dosages adopted for the study.

S. No	Soil Sample	Biopolymer Dosage	G (%)	X (%)
1	S1	Virgin	---	---
		1G	1.0	---
		2G	2.0	---
		1X	---	1.0
		2X	---	2.0
		1G + 1X	1.0	1.0
2	S2	Virgin	---	---
		1G	1.0	---
		2G	2.0	---
		1X	---	1.0
		2X	---	2.0
		1G + 1X	1.0	1.0

3.3. Mixing Strategy

The soil samples that were chosen for analysis were dried in an oven and given some time to cool. Dry or wet mixing methods can be used to mix the selected biopolymers into the soil. In the dry mixing, biopolymers will be added to the dry mass of soil before the addition of water. In wet mixing, a homogeneous solution of biopolymers with deionized is prepared and added to the soil matrix [28]. Dry mixing of biopolymers was preferred in this investigation as wet mixing leads to poor workability when mixed on a large scale. To determine the compaction characteristics and unconfined compressive strength, Biopolymers were added to soils S1 and S2, as stated in Table 3, and allowed to mellow for 24 h. Mellowing permits biopolymers to diffuse uniformly into the soil matrix and promotes the formation of hydrogels.

3.4. Atterberg's Limits

Oven-dried soil passing through sieve no. 40 was tested for its liquid limit and plastic limit using the liquid limit device. Soils mixed with biopolymers at all the enumerated combinations were tested to determine their Atterberg's limits as per ASTM D4318-17el [36].

3.5. Compaction Characteristics

Soil samples added with the selected biopolymers at different proportions were allowed to mellow for 24 h. Lightweight standard proctor compaction tests were conducted on all the soil combinations as per ASTM D698-12 [37]. Soil compaction characteristics such as OMC and MDD values were determined using the standard test procedure.

3.6. Unconfined Compression Strength

The simplest way to assess how effective a soil stabilization approach is to evaluate the soil's compressive strength. In line with ASTM D2166/D2166M-16 [38], soil samples were prepared with a density of MDD and a water content of OMC. Soil samples were tested at a strain rate of 1 mm/min up to a maximum axial strain of 5%. After a curing period of 14, 28, and 60 days, the compressive strength of soil samples was calculated.

3.7. Scanning Electron Microscopy

To evaluate the effectiveness of the employed stabilizer, it is necessary to examine the microstructural organization of soil particles following stabilization. Soil samples treated with biopolymers were examined using Scanning Electron Microscopy (SEM) (Hitachi, Tokyo, Japan; Oxford instrument, Oxford, UK), and SEM images were acquired.

3.8. Embodied Energy in the Production of Guar and Xanthan Gum

Estimating the carbon footprint of a material is necessary to use that for field applications. Carbon footprint print involves the determination of total greenhouse gases in terms

of equivalent CO₂ emissions released into the environment from its production to utility stages. Material with more carbon footprint causes an adverse impact on the environment and is not suggestable as a soil stabilizer. In the present study, CFA was carried out for the selected biopolymers and found that these materials have less carbon footprint compared to conventional materials. Therefore, they could be adopted as effective soil stabilizers. Life cycle analyses (LCA) for both G and X were conducted to calculate the embodied energy during their production. Embodied carbon factor (ECF) was calculated for both the biopolymers used for the investigation.

4. Results and Discussions

4.1. Atterberg's Limits

The liquid and plastic limits of soil S1 and S2 were 63.2%, 30.9% and 48.1%, 25.9% respectively. The addition of biopolymer (G or X) altered the liquid limit (w_L) and plastic limit (w_p) of both soils S1 and S2 used for the investigation. At 1G dosage, w_L increased by 90% and 53% for S1 and S2, respectively. An increase in the w_L is attributed to the formation of a hydrogen bonding network by absorbing more water. No significant increment in w_L was observed when the dosage of G increased to 2%. Soils treated with 1% X also showed an increment in w_L values by 63% and 49% for S1 and S2, respectively. A similar trend of rise in Atterberg's limits of the soil after the addition of biopolymers was observed by the researchers [18,39]. Figure 1 reveals that the effect of X on w_L of both soil S1 and S2 is less significant compared to G, and the same outcome was observed in the earlier research works [35,39]. It is attributed to the reduced degree of linking of X due to the increase in the net negative charge of soil [1]. The increment of X dosage to 2% in the S1 and S2 increased both w_L and w_p values moderately. Later, G and X were cross-linked and added to the soil as per the dosage mentioned in Table 3. Interestingly, the w_p of S2 increased slightly, and it resulted in the reduction in PI to 41.31%, which is lower than the optimum dosages of individual biopolymers. It is attributed to the complex behavior of hydrogel formed by the cross-linking of biopolymers with S2. A similar effect of the rise in the w_p was not observed in the S1, and it can be attributed to the structural arrangement of clay particles. Reduction in w_L was observed in both S1 and S2 when biopolymers were cross-linked. Figure 1. demonstrates how the biopolymer cross-linking raised the w_p of S2 and further regulates PI. When soil is treated with a biopolymer, low-plastic soil becomes medium-plastic, and medium-plastic soil becomes high-plastic soil [38]. Furthermore, the liquid limit is the amount of water required to reduce the undrained shear strength of soil to a specific value; it is understood that at a given water content, the biopolymer-treated (X or G) soil had greater undrained shear strength than the untreated soil [1]. The rise of Atterberg limits of soil after the addition of biopolymers contrasted with that of traditional stabilizing agents, such as cement, lime etc.

The increase in Atterberg's limits of soils after the inclusion of biopolymers is attributed to the natural chemical properties of the biopolymers and the chemical interaction that the clay particles undergo with them. After adding biopolymers to the soil, hydroxyl ions of the biopolymer interact with the pore water available in the soil matrix and increase its viscosity, which can be attributed to the increase in the w_L . Later, clay particles and biopolymer chains interact with each other and form soil agglomeration, which tends to reduce the overall surface area, and the w_L of soil reduces [40]. The combination of the preceding two interactions controls the final w_L of soil. G, being a neutral polysaccharide, interacts with pore water, which increases viscosity and increases the w_L . Due to this, soils treated with G will have high w_L values compared to X. A similar effect of G on the w_L was observed in the research works carried out by earlier researchers [1,18]. When the biopolymers were cross-linked into the soil matrix, Atterberg's limits were increased to some extent and not as much as when the biopolymers were individually added. Limitations on individual usage of biopolymers can be overcome with cross-linking, and it is already being widely used in the food and pharmaceutical industries.

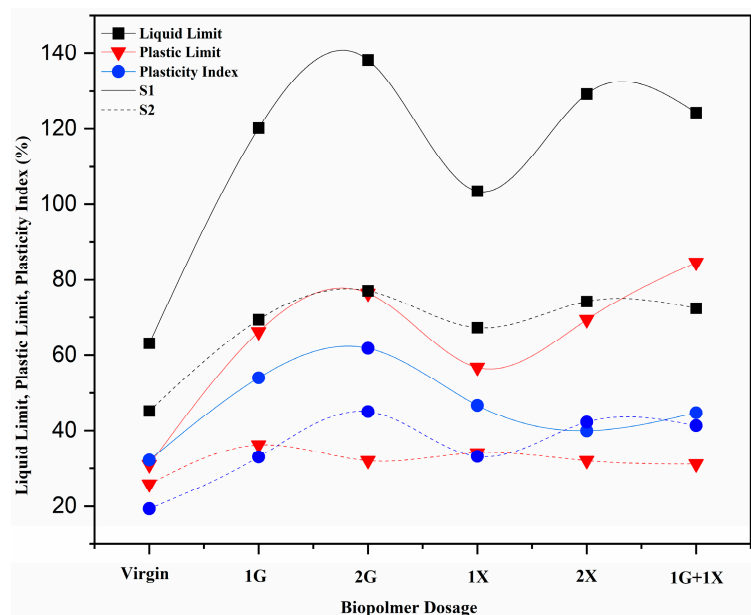


Figure 1. Variation of Atterberg's limits for soil S1 and S2 at different biopolymer dosages.

4.2. Compaction Characteristics

Figure 2 shows the variation of OMC for S1 and S2 at different biopolymer dosages. At 1G dosage, OMC increased by 19% and 36% for S1 and S2, respectively. It can be attributed to the hydrophilic nature of biopolymer, which increases the absorption of water and leads to an increment of OMC. The addition of G to the soil results in the rise of OMC, and the same phenomenon was reported by the researchers [1,18]. X-treated samples also showed an increase in OMC but not as much as compared to that of G-treated. The difference in the phenomena observed is attributed to the complex behavior of X with soil particles, and it is supported by the results of Atterberg's limits. At 2% dosage, both X and G biopolymers showed a proportionate increment in OMC, which can be observed in Figure 2. Contrary to this, results of S1 and S2 at 1G + 1X biopolymer dosage showed a reduction in the OMC by 18% and 14%, respectively, compared to the 2G and 2X dosages of biopolymers. It is attributed to the behavior of hydrogel formed after cross-linking the X and G.

MDD of virgin soils S1 and S2 were 14.41 kN/m^3 and 19.22 kN/m^3 respectively. MDD of S1 at 1G biopolymer dosage was reduced to 13.63 kN/m^3 and 17.82 kN/m^3 for S2. A similar trend of reduction in MDD was observed at 1X dosage for both soils S1 and S2. Irrespective of the biopolymer used, the reduction in MDD is attributed to the increased dosage of biopolymer (from 0% to 1%), which forms a hydrogel filling the voids around the soil particles. This results in high stiffness of the soil matrix and offers more resistance to the applied compaction effort. With an increase in the biopolymer dosage to 2X and 2G, MDD was further reduced, and the same can be observed in Figure 3. However, treatment at 1G + 1X dosage showed a slight increment in MDD of S1 and a decrement in S2 when compared to the biopolymer dosage of 2X. Biopolymer at 2X dosage was found to be effective in controlling the compaction characteristics of soils, but the high embodied energy associated with production may limit its usage in higher dosages.

The mechanism underlying the interaction of clay particles with water and biopolymers is depicted in Figure 4. Following the addition of water to clay, the water interacts with the clay particles and forms a thin layer around them. Clay particles reorganize from a flocculated to a dispersed structure when the compaction was performed wet of optimum. Therefore, the volume decreases, and the density increases. In contrast, when biopolymers are introduced, biopolymers react with water to form a three-dimensional network known as a hydrogel. This hydrogel gets wrapped around soil particles and partially replaces the soil matrix. When a compaction effort is applied to biopolymer-amended soil, the hydrogel resists it by sharing and diffusing the force among the soil particles. Therefore,

the maximum dry density of biopolymer-amended soils will be lower than that of virgin soil or soil stabilized with stabilizing agents such as cement, fly ash, etc.

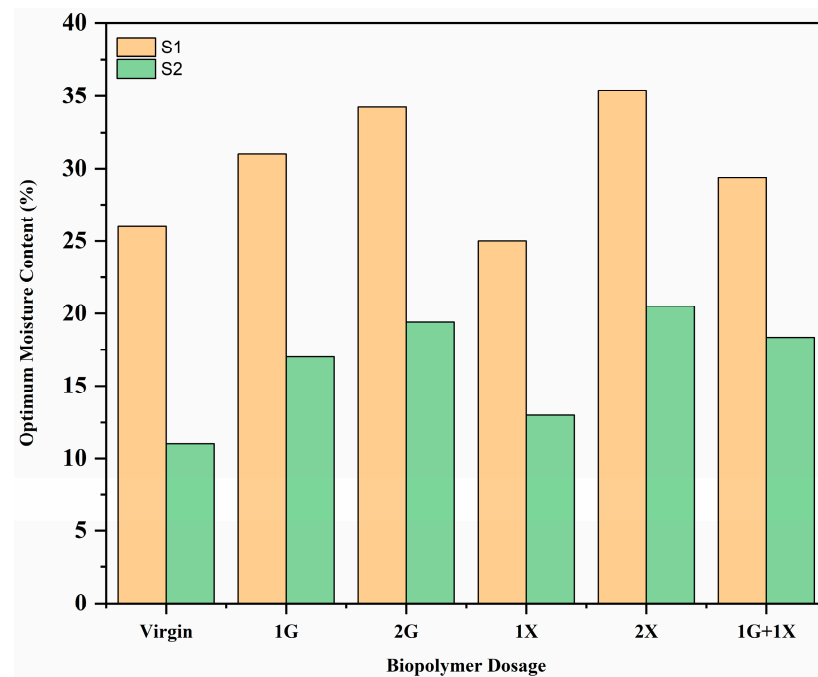


Figure 2. Variation of Optimum Moisture Content (OMC) for soil S1 and S2 at different biopolymer dosages.

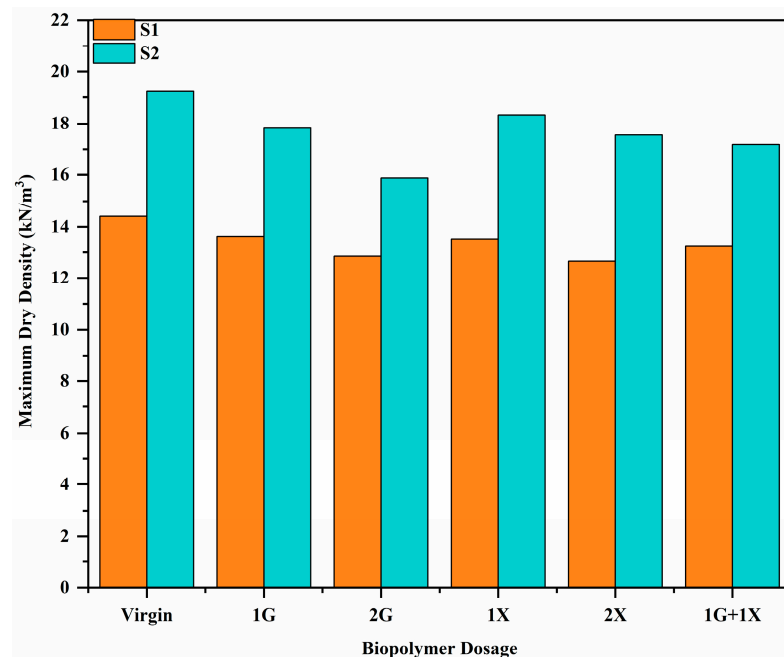


Figure 3. Variation of Maximum Dry Density (MDD) for soil S1 and S2 at different biopolymer dosages.

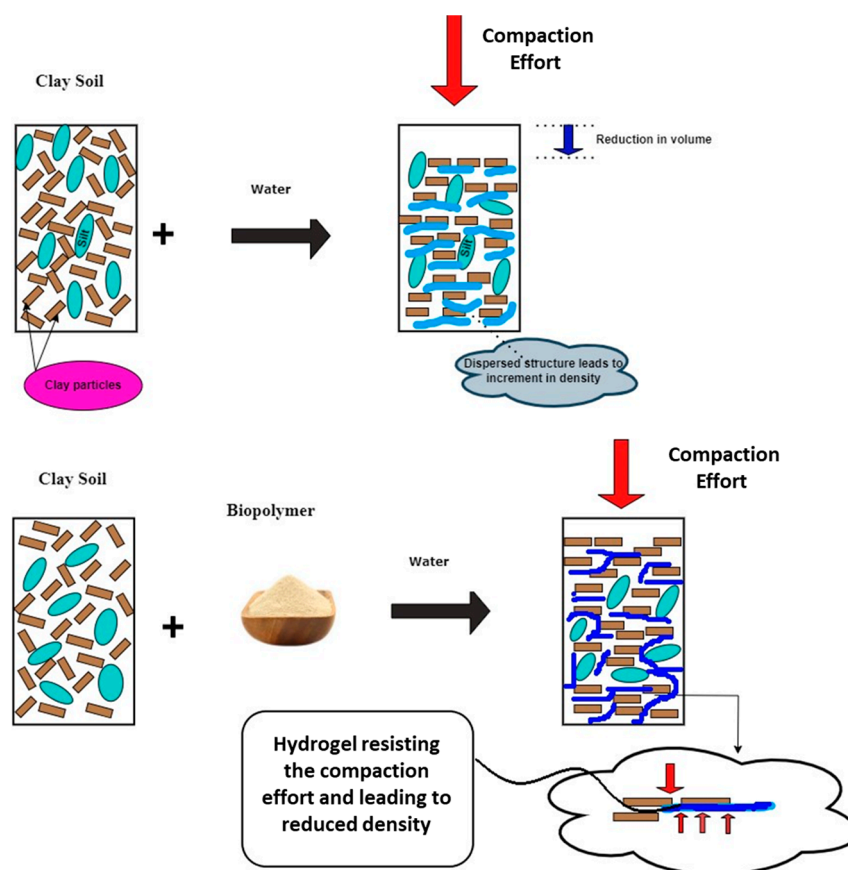


Figure 4. Mechanism of biopolymer interaction with soil particles.

4.3. Unconfined Compression Strength (UCS)

Both S1 and S2 were tested for their UCS on the day of sample preparation, and the values were 92.18 kPa and 121.6 kPa, respectively. Samples made from virgin, G, and X-treated S1 and S2 were cured and tested at the age of 14, 28, and 60 days. Results reveal that the enhancement in UCS of virgin soils S1 and S2 is very minimal. Figure 5 depicts that the UCS of 1G and 1X treated soil samples increased by around 30% for both S1 and S2 at a curing period of 14 days. A substantial enhancement in the UCS of S1 and S2 at the age of 28 days curing period was noticed. It is attributed to the conversion of hydrogel from a rubbery state to a glassy state on drying, and the same phenomenon was observed by the authors who carried out the research on soil stabilization using G and X biopolymers [18]. G and X cross-linked samples of S1 and S2 have shown a considerable increase in UCS at all the curing periods compared to all other individual biopolymer dosages. At the end of the 60-day curing period, the UCS of S1 and S2 treated with crosslinked biopolymers were 209.88 kPa and 283.41 kPa, respectively. It is attributed to the dense agglomeration of soil particles after the biopolymer cross-linking, which is supported by the SEM images from Figures 6 and 7. Results showed that enhancement in UCS for the 2X dosage is close to that of the 1G + 1X dosage. Increasing the X biopolymer dosage may result in better enhancement of UCS by following a suitable curing method. However, the high ECF of X hinders the sustainability aspect of an infrastructure project. Cross-linking of biopolymers addresses the problems associated with the use of individual biopolymers in soil and can be encouraged to increase strength and promote sustainability.

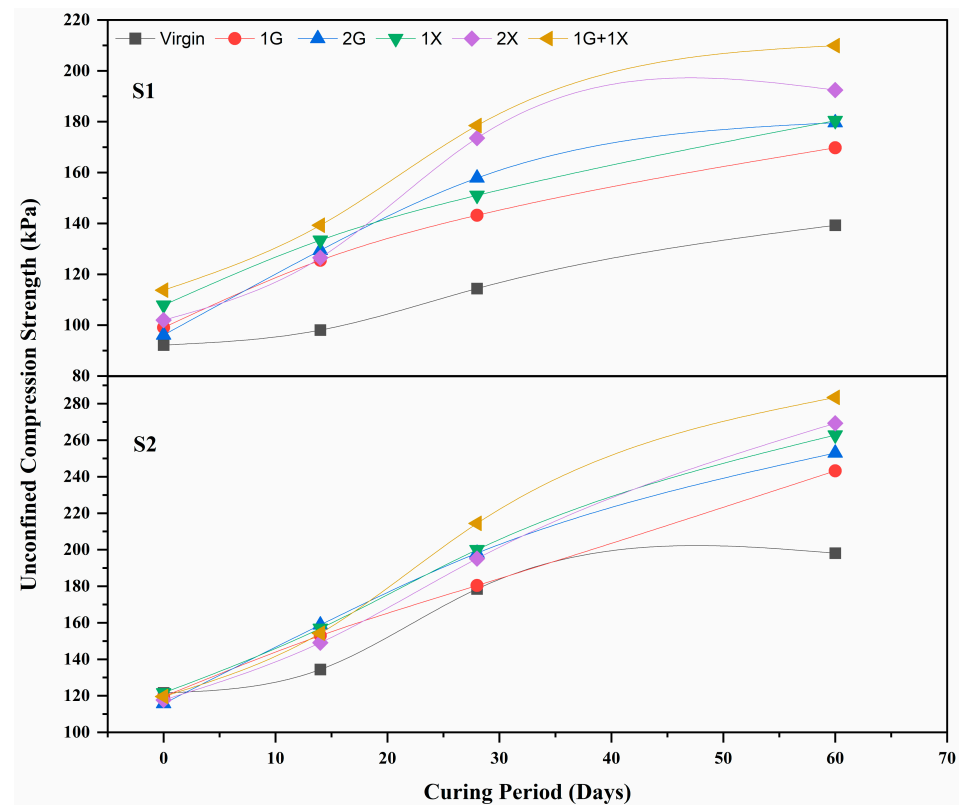


Figure 5. Variation of Unconfined Compression Strength at different curing periods for soil S1 and S2.

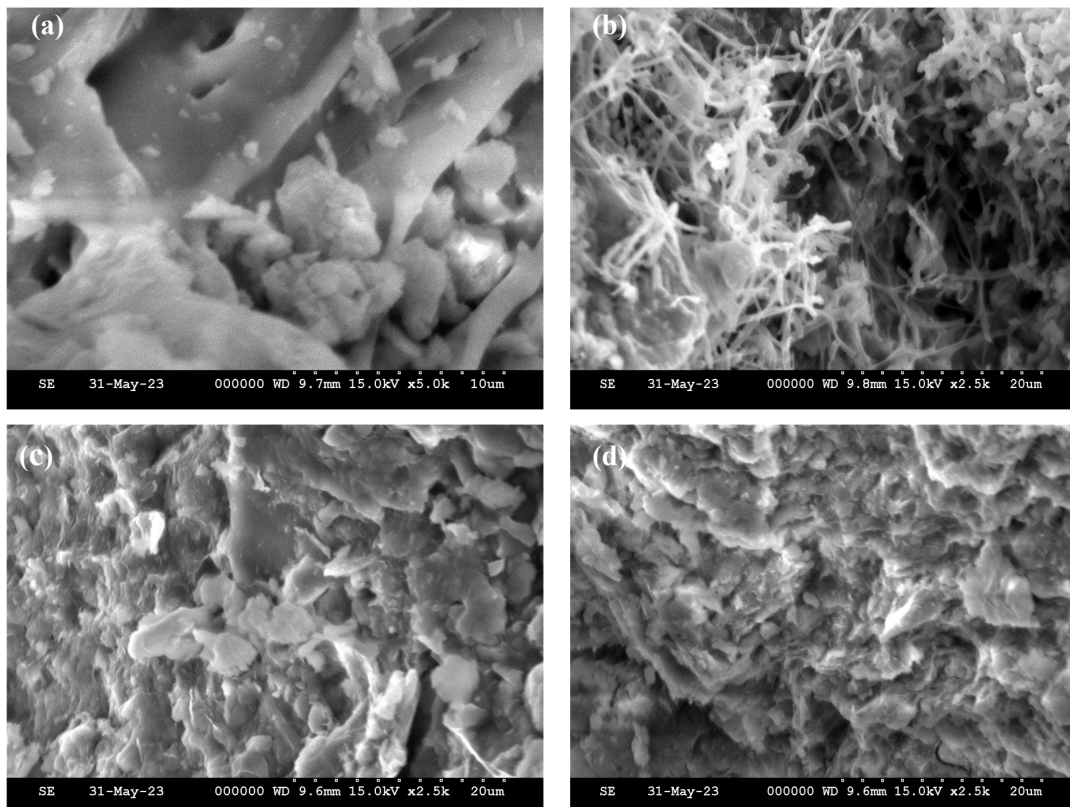


Figure 6. SEM images showing changes in the microstructure arrangement of 28 days cured sample of soil S1 (a) Virgin soil (b) 2G (c) 2X (d) 1G + 1X.

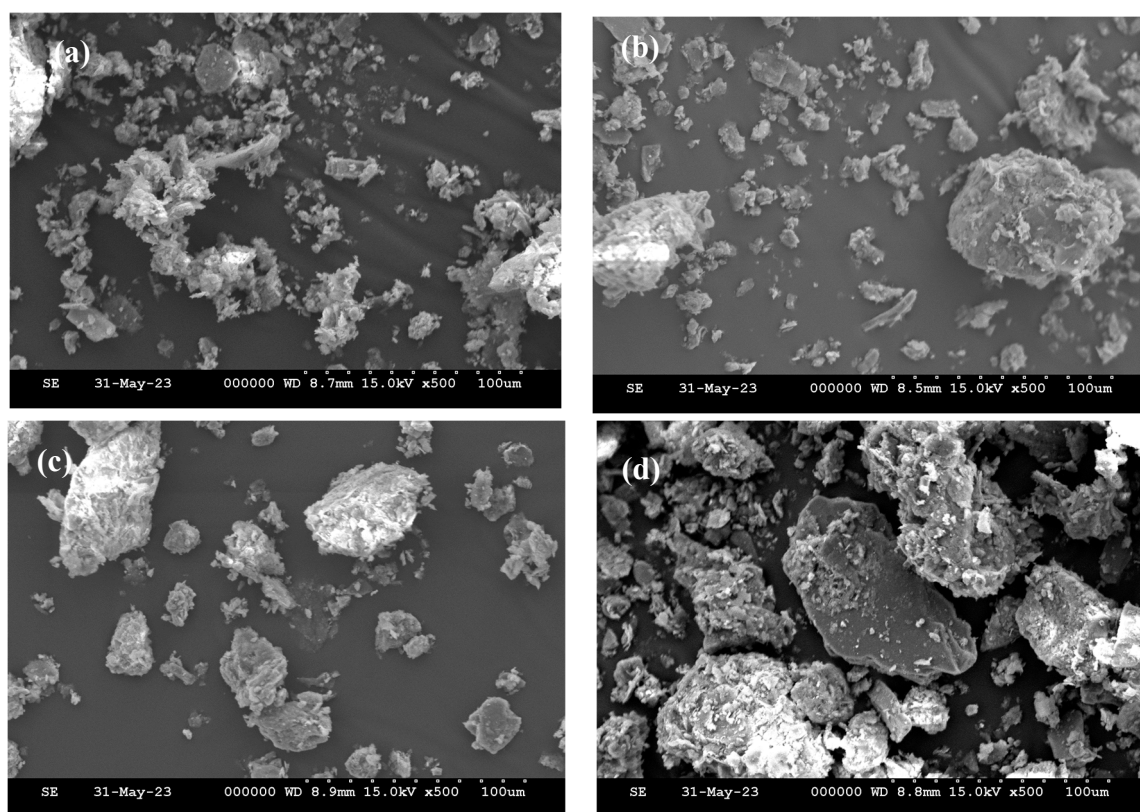


Figure 7. SEM images showing changes in the microstructure arrangement of 28 days cured sample of soil S2 (a) Virgin soil (b) 2G (c) 2X (d) 1G + 1X.

4.4. Structural Electron Microscopy (SEM)

4.4.1. S1

Figure 6 depicts the morphology of the microstructural arrangement of soil particles 28 days after the addition of biopolymer. Figure 6a indicates that the structure of the virgin soil is fragmented and contains some apertures. Images of soil treated at 2G dosage indicate that there are fibers connecting soil particles, as well as some void spaces. It is evident from the image in Figure 6c that the microstructural arrangement became more compact, which may have contributed to the increase in compressive strength. SEM image from Figure 6d reveals that both G and X had a coupled effect on soil S1. There are visible fibers connecting particulates, and the arrangement became denser compared to virgin soil. SEM images confirm the accumulation of hydrogel on the soil surface, and it enhances the soil and biopolymer aggregation. Due to electrically charged clay grains in the soil fabric, direct interactions (electrostatic or hydrogen bonding) between xanthan gum monomers and clay grains take place. These X monomers improve the contact area between grains by forming interconnected cation bridges, thickening the gel that covers the surfaces of the grains, and covering their surfaces [41].

4.4.2. S2

Figure 7 depicts SEM images of the alteration in the microstructural arrangement of soil S2. The image in Figure 7a demonstrates that the soil particles vary in size and are haphazardly dispersed. With the addition of G at 2%, the soil particles adhered to one another, and hydrogel could be the cause. It can be seen in Figure 7c that X had a slightly greater agglomeration effect on the soil particles. Due to the cross-linking effect of both G and X, dense and intense agglomeration of soil particles can be observed in biopolymer cross-linked soil samples. Hydrogel gets coated over the soil grains and helps in the agglomeration of soil particles, and SEM images of biopolymer-treated soil samples confirm the same.

4.5. Fourier-Transform Infrared Spectroscopy (FTIR)

Figure 8 shows the variation of the FTIR spectrum for the virgin S1, 2G, 2X, and 1G + 1X biopolymer dosages. Functional groups ranging from 3971–3700 cm^{-1} in the virgin soil disappeared in all the biopolymer-treated samples. The peak at 3602.38 cm^{-1} corresponds to OH stretching, and the peak has altered marginally in the 2G sample. In 2X and 1G + 1X samples, a significant variation in the peaks of OH stretching was observed. The peak at 1451.17 cm^{-1} denotes C-H bending, and it was broad in virgin soil. In all the biopolymer-treated samples, the peak intensity of C-H bending is sharp and strong. Peak intensity of 749.20 cm^{-1} represents Si-O stretching, and it disappeared in 2X treated soil samples. Variations of FTIR frequencies for S1 at different biopolymer dosages are presented in Table 4.

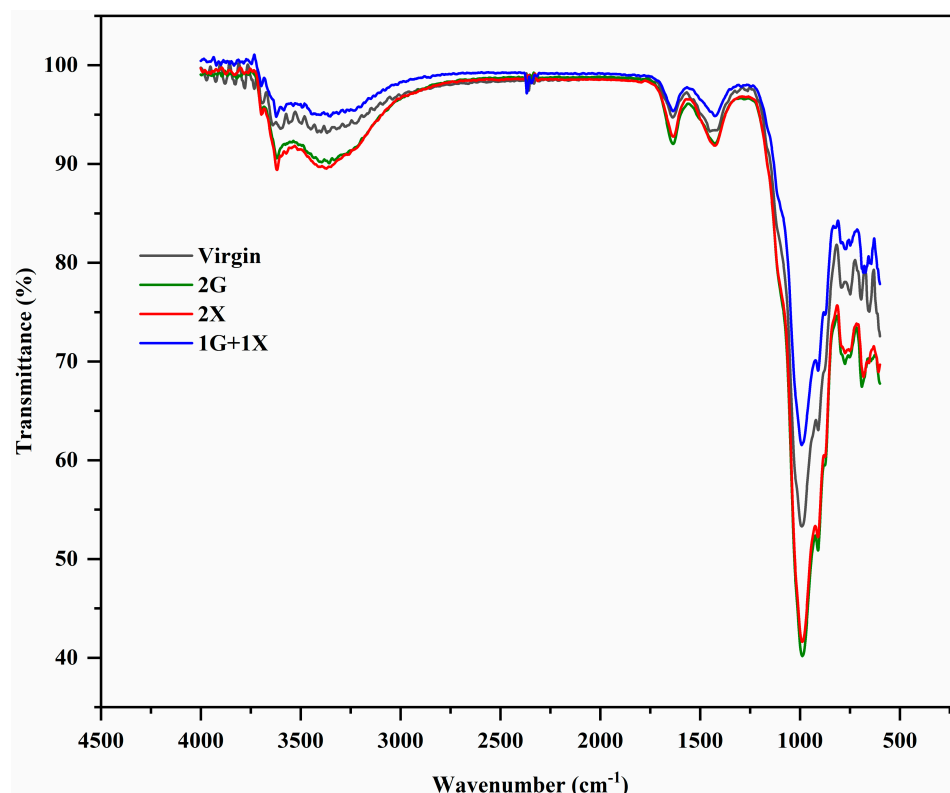


Figure 8. Variation of FTIR frequencies for soil S1 at different biopolymer dosages.

Table 4. Observed FTIR frequencies and band assignments for soil S1 treated at different biopolymer dosages.

Virgin	Characteristic Group	2G	2X	1G + 1X
3700–3971	----	Absent	Absent	Absent
3602.38	OH Stretching	3619.09	3690.12, 3618.77	3689.16, 3618.77
3368.07	N-H Stretching	3356.5	3371.92	3351.68
2357.55	O=C=O Stretching	2365.26	2346.94	2368.16
1638.23	C=C Stretching	1635.34	1634.38	1636.3
1451.17	C-H Bending	1427.07	1426.1	1426.1
991.23	Si-O Stretching in Plane	988.33	989.30	991.23
749.20	Si-O Stretching of Silica	775.24	774.27	770.42

The FTIR analysis of virgin soil S2, 2G, 2X, and 1G + 1X biopolymer dosages can be seen in Figure 9. The frequency ranges are measured as wave numbers ranging from 4000 to 500 cm^{-1} . The peak at 3689.16 cm^{-1} in virgin soil corresponds to O-H stretching due to water. The intensity of this peak is reduced in both X and G treated samples and increased

in the 1G + 1X treated sample. The peak of 2369.12 cm^{-1} in virgin soil denotes O=C=O stretching, and the intensity of the peak is altered in all the biopolymer dosages. The peak at 1632.45 cm^{-1} in virgin soil corresponds to C=C stretching, and it disappears in 2G and 1G + 1X samples. A peak at 1400.07 cm^{-1} denotes O-H bending, and the intensity was reduced in 2G treated samples. The peak intensity of O-H bending was broad and strong in 2X and 1G + 1X treated samples. A peak of 1110.8 cm^{-1} corresponds to C-F stretching, and it disappears in 2G and 1G + 1X samples. Table 5 shows the variation of FTIR frequencies for the soil S2 at different biopolymer dosages.

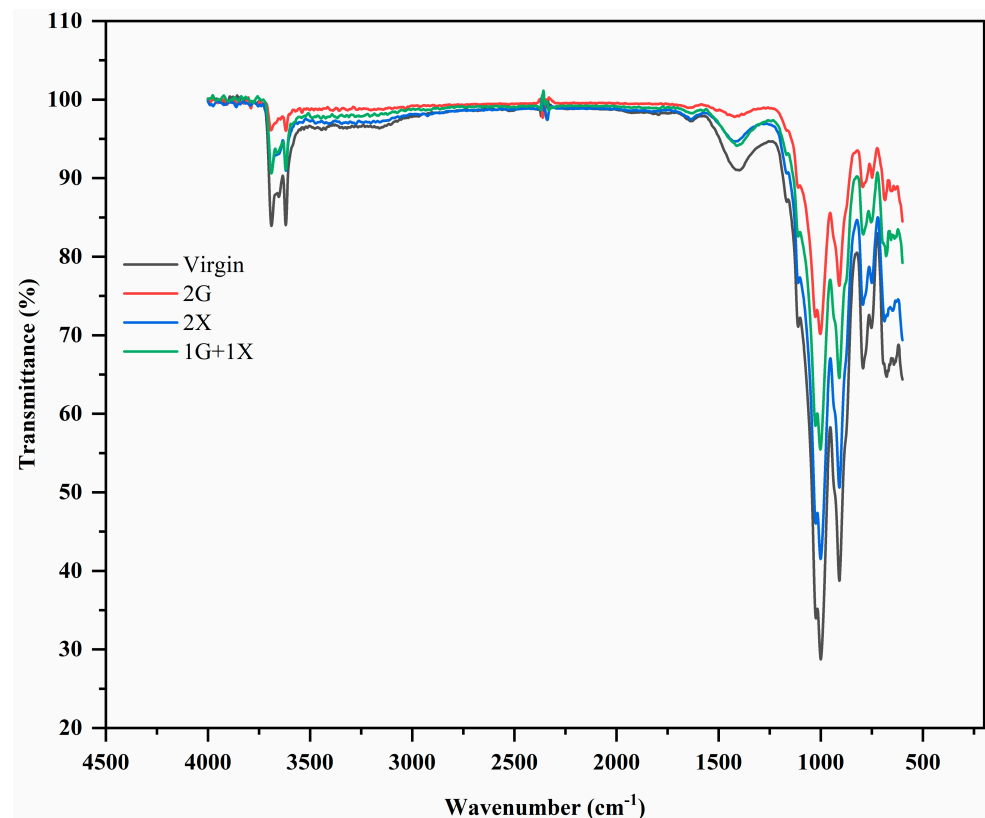


Figure 9. Variation of FTIR frequencies for soil S2 at different biopolymer dosages.

Table 5. Observed FTIR frequencies and band assignments for soil S2 treated at different biopolymer dosages.

Virgin	Characteristic Group	2G	2X	1G + 1X
3689.16, 3619.73	OH Stretching	3691.09, 3618.77	3690.12, 3618.77	3689.16, 3618.77
2369.12	O=C=O Stretching	2361.41	2338.27	2331.52
1632.45	C=C Stretching	Absent	1635.34	Absent
1400.07	O-H Bending	1422.24	1425.14	1411.54
1110.8	C-F Stretching	Absent	1110.8	Absent
1024.02	Si-O Stretching in Plane	1026.9	1024.98	1025.94
793.564	Si-O Stretching of Silica	794.52	794.52	792.6

FTIR analysis shows that significant deviations in ions and elements are responsible for the modification of geotechnical properties of soils S1 and S2 treated at different biopolymer dosages. The presence of the carboxyl group (COOH^-) in X and the hydroxyl group (OH^-) in G was identified through FTIR analysis of the biopolymers. The negatively charged clay surface (OH^-) and anions (COO^-) of X are bridged by monovalent cations (H^+) after the dissolution of X in water, binding the soil particles and providing intergrain resistance [1].

4.6. Embodied Energy in the Production of Guar and Xanthan

This article focuses on the estimation of CO₂ emissions from the production of G and X biopolymers. A quantitative method for calculating the impact of any product from the beginning to the end is life cycle analysis (LCA). However, this method needs a primary database, which is frequently challenging to get, to produce accurate findings. Considering this, the current study assesses CO₂ emissions across the various steps of manufacturing particular biopolymers. The accessible database from the existing literature has been used to estimate CO₂ emissions, subject to boundary constraints. The parameters or circumstances used at each stage of manufacturing are in line with the best yield of certain biopolymers.

4.7. Methodology Adopted

The steps taken to calculate CO₂ emissions for G and X are outlined below:

- Manufacturing phases were identified during the production of unit quantity biopolymer (G/X).
- The amount of electricity required (in kilowatt-hours) to produce an intermediate product at each stage is represented as the amount of energy consumed (in kWh).
- Emission factors for each intermediate product were determined based on the availability of relevant data.
- Based on these emission parameters, CO₂ emissions during the production of one tonne of biopolymer (G/X) were calculated.

4.8. Boundary Conditions

The CO₂ emissions from the following operations are excluded as boundary conditions.

- Human energy inputs.
- Production and transport of fuel used in the project.
- Manufacture of capital goods (equipment and vehicles).
- Transport of raw materials used during the manufacturing stages.
- Cultivation of guar and transportation of seeds to conversion unit (applicable for G only).

4.9. Evaluation of CO₂ Emissions of Guar Gum at the Manufacturing Stage

G undergoes multiple phases of production because it is derived from leguminous vegetation. The first stages are the cultivation and production of guar seeds. The gathered seeds are transported to a processing facility where they are transformed into guar gum. In this investigation, the CO₂ emissions associated with producing G from guar seed at the processing facility are evaluated. Figure 10 depicts the different stages in the production of guar gum and the dotted line represents the system boundary selected for the present study.

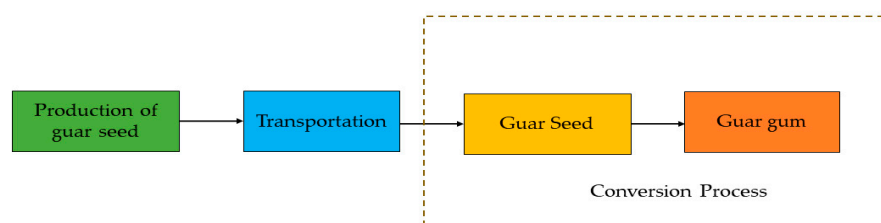


Figure 10. Different stages in the production of guar gum [42].

Figure 11 depicts the germ, endosperm, and husk components of the resultant seed structure. Figure 12 depicts the general process flow of converting G seeds to G at the processing facility. The collected seeds are passed through a shaker to remove 9% of excess material. The seeds are then separated along the germline, processed to remove the “germ,” and utilized as an animal feed byproduct [43]. The moisture content of the halves is increased to 50–60% by weight by heat treatment (Source: US4269975A). At

this moment, it takes 15 min to raise the temperature from 20 °C to 80 °C. To acquire dehusked guar segments, the endosperm and husk must be separated. By hydrating these guar splits for roughly 90 min, their final mass-based moisture content is enhanced to 45%. After being dried at 425 °C, hydrated splits are pulverized to obtain a powder of uniform particle size. The equipment employed in the processing facility of G is identified using the manufacturer’s database and the existing literature. Table 6 provides the energy requirements (in kWh) for each stage.

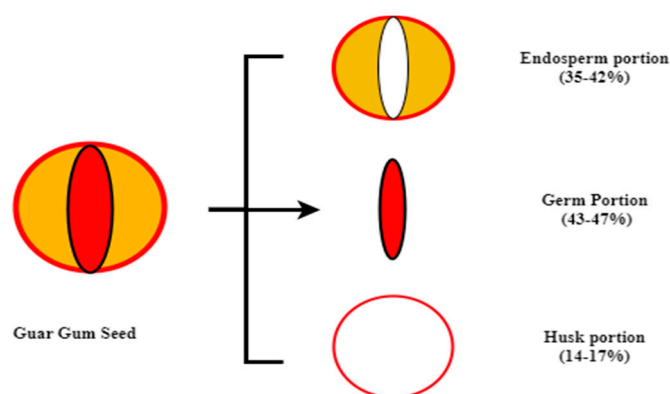


Figure 11. Seed structure of Guar Gum [42].

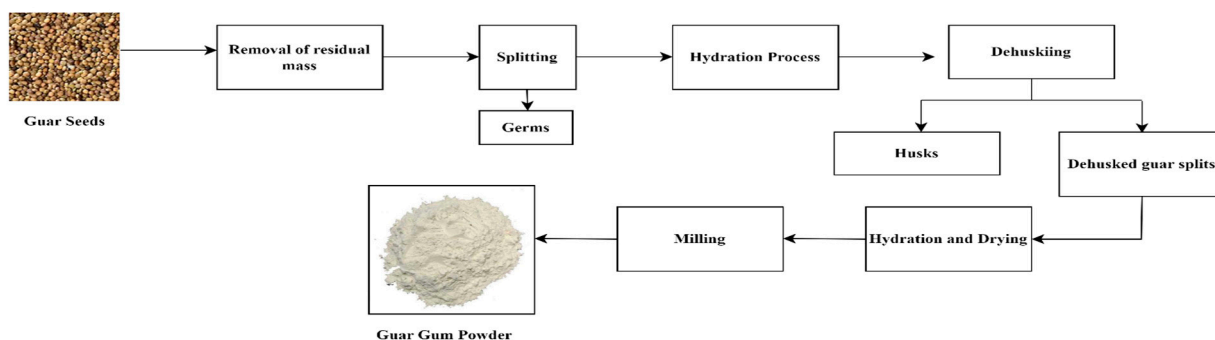


Figure 12. Outline of the guar gum manufacturing process [42].

Table 6. The energy requirement to produce Guar gum (per tonne).

Description	Energy Required kWh
Removal of residual mass (9%)	
Air conveyor	2.71
Shaker table power	0.3
Breaking of seeds through the germ line	
Pneumatic conveyor for moving the seeds to milling equipment	1.375
Hammer mill power to separate germ (1500–1800 rpm)	5
Polish machine	1.65
Passing this through screens to remove the granular meal (germ)	
Sifter (10-mesh screen)	0.3
Heat treatment	
At this stage, the temperature is quickly raised to 80 °C for 15 min	8
Screw conveyor power	0.39
Agitator power	0.37
Hopper power	0.53
Separation of endosperm and husk	
Pneumatic conveyor	1.375
Sifter to remove husk portion	0.3
Hydration of guar splits for 90 min in a slow-turning conveyor (initial 20% and final 45%)	5

Table 6. Cont.

Description	Energy Required kWh
Drying of splits at 425 °C (spray drying)	71.11
Milling to get fine powder	
Hammer mill	5
Pneumatic conveyor to transport these to sifters	1.375
Sifters are used to collect desired guar powder (40–250 mesh)	0.3
Total electricity consumed to produce one tonne of G	105.085 kWh

(Data from manufacturers: Ultrafine gums, Raj Process Equipment and Systems Pvt Ltd., and MV Industries, India).

Therefore, CO₂ emissions (in tonnes) to produce 105.085 kWh or 0.106 MWh of electricity = $0.82 \times 0.106 = 0.087$ per tonne of G.

4.10. Evaluation of CO₂ Emissions of Xanthan Gum at the Manufacturing Stage

X is generated by the bacterium *Xanthomonas campestris* (L strain type) by fermenting glucose and sucrose. Figure 13 depicts the outline of the xanthan gum manufacturing process.

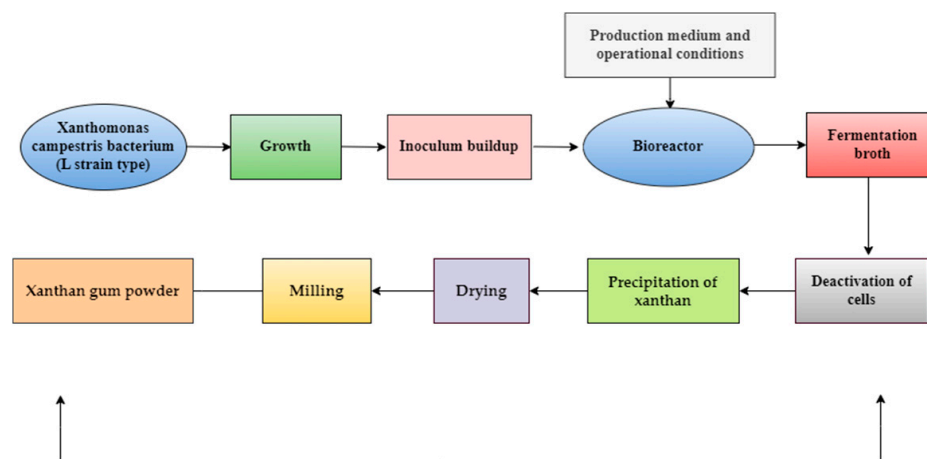


Figure 13. Outline of the xanthan gum manufacturing process [44].

The key steps in the production of xanthan are:

- Culture preservation and growth
- Inoculum buildup
- Production stage
- Recovery of Xanthan gum

The optimum production rate of X depends on culture growth conditions, the type of bioreactor used, the composition of the production medium, and other factors. By adopting appropriate specifications at each stage, the CO₂ emissions are evaluated for optimum X production.

4.10.1. Culture Preservation and Growth

Since it contains more pyruvate, the bacterium '*Xanthomonas Campestris*—L strain' is used to produce the highest xanthan yield. On YM agar (yeast malt agar), a solid medium, the bacteria are grown for 18–20 h at 25–30 °C. Earlier studies [44] determined that a growth temperature of 28 °C was optimum for the development of cultures in the selected media.

4.10.2. Inoculum Buildup

The purpose of inoculum buildup is to increase cell concentration and growth while preventing the production of X. In this phase, the microorganism is transferred from a solid medium to a 100 mL volume of complex liquid medium containing inorganic salts. It is

then subjected to an incubation temperature of 37 °C for 7 h to hinder the production of X [45].

4.10.3. Production Stage

The production stage is typically conducted in a 100 L stirred tank bioreactor with a two-step fermenter (batch mode of operation) in two steps [44,46]. In the first step, the optimum impeller speed in the tank is 200 rpm for 12 h; in the second step, the optimum impeller speed in the production fermenter is 600 rpm for 60 h (pH = 7). A 1 L/L aeration rate is assumed. The temperature for optimum efficiency is considered as 28 °C. The specifications under consideration yield 30 g/L of xanthan. The composition of the production medium is crucial to the yield of X with increased viscosity. Carbon (C) and nitrogen (N) (source) are macronutrients that consist of calcium, iron, and potassium salts. Higher C/N ratios favor the optimum production of X [47]. For optimum X production, the best carbon source is carbohydrates (glucose/sucrose) at a concentration of 2–4% [48] and the best nitrogen source is glutamate at 15 mM. Additionally, modest amounts of organic salts (such as citric acid) boost the production of X. In addition to nitrogen and phosphorus, the presence of magnesium influences the growth of the culture, and sulfur influences the production of X. Table 7 displays the optimum production medium composition used for fermentation (100 L) in this study.

Table 7. Production medium composition for optimum Xanthan gum production (per batch).

Production Medium Composition [44]	Production Medium Required for Fermentation (100 L) (for the Present Study)
Sucrose (40 g/L)	4 kg
Citric acid (2.1 g/L)	210 g
Calcium carbonate (CaCO ₃) (0.020 g/L)	2 g
Ferric chloride (FeCl ₃ 6H ₂ O) (0.020 g/L)	2 g
Concentrated HCl (0.13 mL/L)	13 mL or 15.34 g
Zinc oxide (ZnO) (0.006 g/L)	0.6 g
Boric acid (H ₃ BO ₃) (0.006 g/L)	0.6 g
Magnesium chloride (MgCl ₂) (0.507 g/L)	50.7 g
Sodium sulphate (Na ₂ SO ₄) (0.089 g/L)	8.9 g
Monopotassium phosphate (KH ₂ PO ₄) (2.866 g/L)	286 g
Ammonium nitrate (NH ₄ NO ₃) (1.14 g/L)	1.14 g

4.11. Recovery of Xanthan Gum

The final fermentation broth typically comprises 3±10 g/L of residual nutrients, 1–10 g/L of cells, and 10–30 g/L of X. A higher X concentration makes the broth more viscous and difficult to process, prompting its (i.e., broth's) dilution. As indicated in Figure 13, the main steps involved in the recovery process include cell deactivation, precipitation of X, drying, and grinding. The cells are deactivated using chemical treatment and heat treatment techniques. Chemicals, on the other hand, trigger polymer breakdown by lowering the pyruvate level of the product when added to the broth. Additionally, if enzymes are used, the broth must be cleaned of the enzymes, adding to the overall expense. The preferred approach for deactivating cells is thermal treatment, which involves pasteurizing broth at the right temperature of 80–130 °C and pH level of 6.3–6.9 for 10–20 min. A highly soluble viscous xanthan colloidal solution is created after thermal treatment. Precipitation of the solution is handled using organic solvents such ethanol (6 vol. per volume of broth), isopropyl alcohol (3 vol. per volume of broth), and tri- or tetravalent salts (calcium, aluminum, quaternary ammonium salts) to recover the xanthan gum.

In the present study, the final product of X from the broth is assumed as 30 g/L or 3 kg/100 L (3 kg per 100 L of fermentation broth). The conditions adopted for thermal treatment are as follows:

- It is assumed that a temperature of 105 °C will cause cells to deactivate.
- pH of 6.6 for 15 min

- For the precipitation of X, isopropyl alcohol (3 vol per liter of broth) is a possibility. For the considered conditions, 300 L or 240.9 g of isopropyl alcohol is required per batch.
- Drying of precipitated X is considered to take place under a vacuum temperature of 55 °C for 12 h.
- The optimum speed adopted for milling the dried X is 200 rpm for a period of 2 h.

Table 8 shows the amount of energy used by the equipment at each stage of the X production process (measured in kWh of electricity needed). In addition to the emissions by equipment, the manufacturing of production medium accounts for a considerable amount of CO₂ emissions. Considering this, CO₂ emissions are assessed for the X production medium composition and presented in Table 9. According to the CO₂ baseline database for the Indian power sector (Source: Ministry of Power Central Electricity Authority, India), the CO₂ emission factor (in tonnes) to create 1 MWh of electricity is taken as 0.82.

Table 8. Energy is consumed in each stage in terms of electricity required (in kWh).

Stage	Energy Required (kWh) (per Batch)	Remarks
Culture growth	----	Since the energy spent is not considered to evaluate CO ₂ emissions at this stage, room temperature is assumed to be 28 °C, which offers optimum conditions for the growth of microorganisms.
Incubation stage	0.06	Temperature 37 °C; time 7 h (HettCube incubator of 535 × 690 × 1419 mm size is considered)
Production stage	0.084	First step: speed of impeller 200 rpm for 12 h [49]
	1.08	Second step: speed of impeller 600 rpm for 60 h [49]
Recovery of X	2.1	Deactivation of cells: temperature 105 °C, pH 6.6 for 15 min
	0.071	Drying of precipitated X: temperature 55 °C for 12 h
	0.015	Milling: speed 200 rpm for 2 h
Total electricity required (I)		3.41 kWh or 3.41×10^{-3} MWh

Table 9. Estimation of CO₂ emissions for production medium composition [50].

Optimal Production Medium Composition	Emission Factor (kg CO ₂ per kg)	CO ₂ Emission (kg Per Batch)
Sucrose (40 g/L)	0.3	1.2
Citric acid (2.1 g/L)	0.41	0.0861
Calcium carbonate (CaCO ₃) (0.020 g/L)	0.4397	0.0008794
Ferric chloride (FeCl ₃ 6H ₂ O) (0.020 g/L)	0.18	0.00162
Concentrated HCl (0.13 mL/L)	0.89	0.01365
Zinc oxide (ZnO) (0.006 g/L)	2.91	0.001746
Boric acid (H ₃ BO ₃) (0.006 g/L)	0.72	0.000432
Magnesium chloride (MgCl ₂) (0.507 g/L)	Not Available	-
Sodium sulphate (Na ₂ SO ₄) (0.089 g/L)	0.47	0.004183
Monopotassium phosphate (KH ₂ PO ₄) (2.866 g/L)	Not Available	-
Ammonium nitrate (NH ₄ NO ₃) (1.144 g/L)	4.09	0.004663
Isopropyl alcohol (3 vol per broth volume)	3.84	0.9216
Total CO ₂ emissions in kg per batch (II)		2.235 kg/3 kg of XG

Therefore, CO₂ emissions (in tonne) to produce 3.41×10^{-3} MWh of electricity = $0.82 \times 3.41 \times 10^{-3} = 2.796 \times 10^{-3}$ per 3 kg of XG (I).

The total CO₂ emissions during the X production (I + II) = 2.235 + 2.796 = 5.02 kg per 3 kg of X or 1.67 t of CO₂ per tonne of X.

- From the existing literature, the CO₂ emissions associated with cement production (including emissions from raw materials) are 2.16 tonnes/tonne of cement [51,52]; for coal combustion, it is 2.86 tonnes/tonne of coal [53,54]; for quick lime (process + combustion + electricity emissions) it is 1.092 tonnes/tonne of quick lime [55].

5. Conclusions

The current study focused on computing the embodied energy of both Guar gum (G) and Xanthan gum (X) from the production stage with boundary conditions. Furthermore, the effect of cross-linking these biopolymers in altering the geotechnical properties of soils exhibiting different plasticity characteristics was investigated, and the following conclusions are drawn from this study:

- The liquid and plastic limits increased for both soils with the addition of selected biopolymers. G had a significant effect on the liquid limit values of soils, and X influenced the plastic limit values.
- The plasticity of soils S1 and S2 increased with the addition of X and G individually, and the cross-linking addressed this issue by decreasing the plasticity index to a good extent. The durability and physical integrity of the hydrogel formed after the addition of biopolymers neutralize the effect of a rise in the plasticity index of soils in the long run.
- The optimum dosage of G is found to be 2% for both S1 and S2, and at this dosage, the optimum moisture content (OMC) increased to 31% and 19.4% compared to their untreated cases. In similar lines, the optimum dosage of X is found to be 2% for both S1 and S2 and at this dosage, the OMC of S1 and S2 increased to 35.4% and 20.5%, which are slightly higher compared to the case of G.
- The maximum dry density (MDD) of virgin soils S1 and S2 were 14.41 kN/m³ and 19.22 kN/m³ respectively. At optimum dosages of G and X biopolymers, MDD of both soils S1 and S2 were reduced to some extent. By cross-linking G and X and adding them to S1 and S2, the OMC reduced, and MDD increased in higher amounts when compared to adding X and G independently at their optimum dosages.
- The unconfined compression strength (UCS) of virgin soils S1 and S2 at the end of the 60-day curing period were 92.18 kPa and 121.6 kPa, respectively. At the same age of curing, the UCS of both soils S1 and S2 with the addition of optimum dosage of G were found to be 179.62 and 253.01 kPa, respectively. This study has further revealed that, at the optimum biopolymer dosage of 2%, the improvement in the UCS of soils S1 and S2 is higher in X-treated samples when compared to that of G-treated ones.
- Enhancement in the UCS of soil samples treated by cross-linking the biopolymers G and X was high compared to the addition of X and G individually at their optimum dosages.
- The SEM images confirmed the coupled effect of both the biopolymers G and X in soils S1 and S2 at the biopolymer dosage of 1G + 1X.
- The FTIR analysis confirmed the presence of hydrogel in the soils treated at all the biopolymer dosages, responsible for the alteration of targeted geotechnical properties.
- The CO₂ emissions for G and X during the manufacturing stage subjected to the boundary conditions are calculated and found to be 0.087 and 1.67, respectively.

This study has revealed that cross-linking of biopolymers addresses the limitations of individual biopolymers, can be efficient in enhancing the targeted geotechnical parameters, and can act as a perfect substitute for the traditional stabilizing agents. Relying more on traditional stabilizing agents, such as lime and cement, results in the rapid exhaustion of natural resources and hampers the environment with their high embodied CO₂ emissions. It is observed that biopolymer production accounts for lesser CO₂ emissions compared to

these conventional materials. Moreover, at the end of service life, the CO₂ released due to biopolymer degradation is reabsorbed by surrounding flora and fauna, maintaining carbon neutrality. Biopolymer cross-linking can be an effective alternative to traditional stabilizers as it facilitates sustainable development in the field of geotechnical engineering. High costs incurred by the usage of biopolymers can be controlled as the availability of biopolymers in the market is expected to rise in the coming future.

6. Potential Research Directions

Biopolymeric soil stabilization is presently an area of active research, which has enormous potential for its environmentally friendly building practices. The potential research applications of these novel materials include:

- Biopolymer composites
- Tailored biopolymer blends
- Assessment of long-term performance and durability
- Field-scale applications
- Multifunctional applications

By targeting the above research directions, the field of biopolymeric soil stabilization can advance toward more sustainable, efficient, and environmentally friendly solutions for construction and land management solutions.

Author Contributions: Conceptualization, methodology, M.A.K. and A.A.B.M.; formal analysis, investigation, M.A.K.; resources, A.A.B.M. and A.A.; data curation, M.A.K., K.V.V. and A.A.B.M.; writing—original draft preparation, M.A.K., A.A.B.M., K.V.V. and A.A.; writing—review and editing, M.A.K., A.A.B.M., K.V.V. and A.A.; visualization, M.A.K.; supervision, A.A.B.M.; project administration, A.A.B.M.; funding acquisition, A.A. All authors have read and agreed to the published version of the manuscript.

Funding: This research was funded by King Saud University through Researchers Supporting Project Number 2023R279, King Saud University, Riyadh, Saudi Arabia.

Data Availability Statement: The data presented in this study are available on request from the corresponding author.

Acknowledgments: The authors would like to thank King Saud University, Riyadh, Saudi Arabia, Researchers Supporting Project Number 2023R279 for funding research.

Conflicts of Interest: The authors declare that the research was conducted in the absence of any commercial or financial relationships that could be construed as a potential conflict of interest.

Nomenclature

Symbol	Definition
G	Guar gum, a galactomannan polysaccharide extracted from guar beans, has thickening and stabilizing properties useful in food, feed, and industrial applications.
X	Xanthan gum is a polysaccharide with many industrial uses, including as a common food additive.
S1	High compressible clay
S2	Medium compressible clay
1G	1% of Guar gum
2G	2% of Guar gum
1X	1% of Xanthan gum
2X	2% of Xanthan gum
1G + 1X	1% of Guar gum + 1% of Xanthan gum (Cross-linked)
OMC	Optimum moisture content (%) the moisture content at which the soil can be compacted to its maximum dry density.
MDD	Maximum dry density (kN/m^3) influences the shear strength, permeability, bearing capacity, and overall stability of soil.
w_L	Liquid limit (%) is the water content where the soil starts to behave as a liquid.
w_P	Plastic limit (%), moisture content at which a fine-grained soil can no longer be remolded without cracking.
PI	Plasticity Index is the difference between liquid and plastic limits is called the plasticity index, and it represents the range of water content over which the soil is plastic.
SEM	Scanning Electron Microscopy is one of the most widely used instrumental methods for the examination and analysis of micro- and nanoparticle imaging characterization of materials.
ECF	Embodied Carbon Factor,
CFA	Carbon Footprint Analysis, calculation of the amount of greenhouse gases (GHG) produced due to human activities, measured in units of carbon dioxide.
EICP	Enzyme-Induced Calcite Precipitate
MICP	Microbial Induced Calcium Precipitate
BPST	Biopolymer Soil Treatment
LCA	Life Cycle Analysis is a systematic analysis of the potential environmental impacts of products or services during their entire life cycle.
FTIR	Fourier-transform infrared spectroscopy

References

1. Vydehi, K.V.; Moghal, A.A.B. Effect of Biopolymeric Stabilization on the Strength and Compressibility Characteristics of Cohesive Soil. *J. Mater. Civ. Eng.* **2022**, *34*, 04021428. [\[CrossRef\]](#)
2. Ahmed, M.; Bashar, I.; Alam, S.T.; Wasi, A.I.; Jerin, I.; Khatun, S.; Rahman, M. An overview of Asian cement industry: Environmental impacts, research methodologies and mitigation measures. *Sustain. Prod. Consum.* **2021**, *28*, 1018–1039. [\[CrossRef\]](#)
3. Abd, S.M.; Mhaimeed, I.S.; Tayeh, B.A.; Najm, H.M.; Qaidi, S. Investigation of the use of textile carbon yarns as sustainable shear reinforcement in concrete beams. *Case Stud. Constr. Mater.* **2022**, *18*, e01765. [\[CrossRef\]](#)
4. Harsh, H.; Moghal, A.A.B.; Rasheed, R.M.; Almajed, A. State-of-the-Art Review on the Role and Applicability of Select Nano-Compounds in Geotechnical and Geoenvironmental Applications. *Arab. J. Sci. Eng.* **2023**, *48*, 4149–4173. [\[CrossRef\]](#)
5. Moghal, A.A.B.; Vydehi, K.V. State-of-the-art review on efficacy of xanthan gum and guar gum inclusion on the engineering behavior of soils. *Infrast. Solut.* **2021**, *6*, 108. [\[CrossRef\]](#)
6. Amulya, G.; Moghal, A.A.B.; Almajed, A. Sustainable binary blending for low-volume roads—Reliability-based design approach and carbon footprint analysis. *Materials* **2023**, *16*, 2065. [\[CrossRef\]](#)
7. Shalchian, M.M.; Arabani, M. Application of plant-derived fibers in soil reinforcement on experimental, numerical, and case study scales: A review. *Bull. Eng. Geol. Environ.* **2023**, *82*, 19. [\[CrossRef\]](#)
8. Moghal, A.A.B. State-of-the-Art Review on the Role of Fly Ashes in Geotechnical and Geoenvironmental Applications. *J. Mater. Civ. Eng.* **2017**, *29*, 04017072. [\[CrossRef\]](#)
9. Amulya, G.; Moghal, A.A.B.; Basha, B.M.; Almajed, A. Coupled Effect of Granite Sand and Calcium Lignosulphonate on the Strength Behavior of Cohesive Soil. *Buildings* **2022**, *12*, 1687. [\[CrossRef\]](#)
10. Raghuram, A.S.S.; Basha, B.M.; Moghal, A.A.B. Effect of fines content on the hysteretic behavior of water-retention characteristic curves of reconstituted soils. *J. Mater. Civ. Eng.* **2020**, *32*, 04020057. [\[CrossRef\]](#)
11. Al-Mahbashi, A.M.; Al-Shamrani, M.A.; Moghal, A.A.B. Soil–water characteristic curve and one-dimensional deformation characteristics of fiber-reinforced lime-blended expansive soil. *J. Mater. Civ. Eng.* **2020**, *32*, 04020125. [\[CrossRef\]](#)

12. Amulya, G.; Moghal, A.A.B.; Almajed, A. A State-of-the-Art Review on Suitability of Granite Dust as a Sustainable Additive for Geotechnical Applications. *Crystals* **2021**, *11*, 1526. [[CrossRef](#)]
13. Onyelowe, K.C.; Ebid, A.M.; Hanandeh, S.; Moghal, A.A.B.; Onuoha, I.C.; Obianyo, I.I.; Ubachukwu, O.A. The influence of fines on the hydro-mechanical behavior of sand for sustainable compacted liner and sub-base construction applications. *Asian J. Civ. Eng.* **2023**, 1–13. [[CrossRef](#)]
14. Sidiq, A.; Robert, D.J.; O'Donnell, B.; Setunge, S.; Swarup, A.; Tostvrsnik, F. Investigation of Enzyme-Based Soil Stabilization in Field Application. *J. Mater. Civ. Eng.* **2023**, *35*, 04023086. [[CrossRef](#)]
15. Seo, S.; Lee, M.; Im, J.; Kwon, Y.M.; Chung, M.K.; Cho, G.C.; Chang, I. Site application of biopolymer-based soil treatment (BPST) for slope surface protection: In-situ wet-spraying method and strengthening effect verification. *Constr. Build. Mater.* **2021**, *307*, 124983. [[CrossRef](#)]
16. EBadakhshan; Noorzad, A.; Vaunat, J. Stabilization of Soft Clays Exposed to Freeze–Thaw Cycles Using Chitosan. *J. Cold Reg. Eng.* **2023**, *37*, 04023004. [[CrossRef](#)]
17. Ayeldeen, M.; Negm, A.; El-Sawwaf, M.; Kitazume, M. Enhancing mechanical behaviors of collapsible soil using two biopolymers. *J. Rock Mech. Geotech. Eng.* **2017**, *9*, 329–339. [[CrossRef](#)]
18. Muguda, S.; Hughes, P.N.; Augarde, C.E.; Perlot, C.; Bruno, A.W.; Gallipoli, D. Cross-linking of biopolymers for stabilizing earthen construction materials. *Build. Res. Inf.* **2021**, *50*, 502–514. [[CrossRef](#)]
19. Almajed, A.; Lemboye, K.; Moghal, A.A.B. A Critical Review on the Feasibility of Synthetic Polymers Inclusion in Enhancing the Geotechnical Behavior of Soils. *Polymers* **2022**, *14*, 5004. [[CrossRef](#)]
20. Acharya, R.; Pedarla, A.; Bheemasetti, T.V.; Puppala, A.J. Assessment of Guar Gum Biopolymer Treatment toward Mitigation of Desiccation Cracking on Slopes Built with Expansive Soils. *Transp. Res. Rec.* **2017**, *2657*, 78–88. [[CrossRef](#)]
21. Xiao, Y.; Ma, G.; Wu, H.; Lu, H.; Zaman, M. Rainfall-Induced Erosion of Bio cemented Graded Slopes. *Int. J. Geomech.* **2022**, *22*, 04021256. [[CrossRef](#)]
22. Hisseini, B.H.A.; Bennabi, A.; Hamzaoui, R.; Makki, L.; Blanck, G. Treatment and Recovery of Clay Soils Using Geopolymerization Method. *Int. J. Geomech.* **2021**, *21*, 04021206. [[CrossRef](#)]
23. Soldo, A.; Miletić, M.; Auad, M.L. Biopolymers as a sustainable solution for the enhancement of soil mechanical properties. *Sci. Rep.* **2020**, *10*, 267. [[CrossRef](#)] [[PubMed](#)]
24. Moghal, A.A.B.; Vydehi, V.; Moghal, M.B.; Almatrudi, R.; AlMajed, A.; Al-Shamrani, M.A. Effect of Calcium-Based Derivatives on Consolidation, Strength, and Lime-Leachability Behavior of Expansive Soil. *J. Mater. Civ. Eng.* **2020**, *32*, 04020048. [[CrossRef](#)]
25. Rasheed, R.M.; Moghal, A.A.B.; Rambabu, S.; Almajed, A. Sustainable assessment and carbon footprint analysis of polysaccharide biopolymer-amended soft soil as an alternate material to canal lining. *Front. Environ. Sci.* **2023**, *11*, 1214988. [[CrossRef](#)]
26. Rasheed, R.M.; Moghal, A.A.B.; Jannepally, S.S.R.; Rehman, A.U.; Chittoori, B. Shrinkage and Consolidation Characteristics of Chitosan-Amended Soft Soil—A Sustainable Alternate Landfill Liner Material. *Buildings* **2023**, *13*, 2230. [[CrossRef](#)]
27. Ayeldeen, M.K.; Negm, A.M.; El Sawwaf, M.A. Evaluating the physical characteristics of biopolymer/soil mixtures. *Arab. J. Geosci.* **2016**, *9*, 371. [[CrossRef](#)]
28. Chang, I.; Cho, G.C. Strengthening of Korean residual soil with β -1,3/1,6-glucan biopolymer. *Constr. Build. Mater.* **2012**, *30*, 30–35. [[CrossRef](#)]
29. Ding, X.; Xu, G.; Liu, W.V.; Yang, L.; Albijan, B. Effect of polymer stabilizers' viscosity on red sand structure strength and dust pollution resistance. *Powder Technol.* **2019**, *352*, 117–125. [[CrossRef](#)]
30. Varaprasad, K.; Raghavendra, G.M.; Jayaramudu, T.; Yallapu, M.M.; Sadiku, R. A mini review on hydrogels classification and recent developments in miscellaneous applications. *Mater. Sci. Eng. C* **2017**, *79*, 958–971. [[CrossRef](#)]
31. Casas, J.A.; Mohedano, A.F.; García-Ochoa, F. Viscosity of guar gum and xanthan/guar gum mixture solutions. *J. Sci. Food Agric.* **2000**, *80*, 1722–1727. [[CrossRef](#)]
32. Umar, M.; Kassim, K.A.; Chiet, K.T.P. Biological process of soil improvement in civil engineering: A review. *J. Rock Mech. Geotech. Eng.* **2016**, *8*, 767–774. [[CrossRef](#)]
33. Thombare, N.; Jha, U.; Mishra, S.; Siddiqui, M.Z. Guar gum as a promising starting material for diverse applications: A review. *Int. J. Biol. Macromol.* **2016**, *88*, 361–372. [[CrossRef](#)]
34. Sharma, G.; Sharma, S.; Kumar, A.; Al-Muhtaseb, A.H.; Naushad, M.; Ghfar, A.A.; Mola, G.T.; Stadler, F.J. Guar gum and its composites as potential materials for diverse applications: A review. *Carbohydr. Polym.* **2018**, *199*, 534–554. [[CrossRef](#)] [[PubMed](#)]
35. Muguda, S.; Booth, S.J.; Hughes, P.N.; Augarde, C.E.; Perlot, C.; Bruno, A.W.; Gallipoli, D. Mechanical properties of biopolymer-stabilized soil-based construction materials. *Géotechnique Lett.* **2017**, *7*, 309–314. [[CrossRef](#)]
36. *ASTM D4318-17e1*; Standard Test Methods for Liquid Limit, Plastic Limit, and Plasticity Index of Soils. ASTM: West Conshohocken, PA, USA, 2017.
37. *ASTM D698-12*; Standard Test Methods for Laboratory Compaction Characteristics of Soil Using Standard Effort (12400 ft-lbf/ft³(600 kN-m/m³)). ASTM: West Conshohocken, PA, USA, 2021.
38. *ASTM D2166/D2166M-16*; Standard Test Method for Unconfined Compressive Strength of Cohesive Soil. ASTM: West Conshohocken, PA, USA, 2016.
39. Nugent, R.; Zhang, G.; Gambrell, R. Effect of exopolymers on the liquid limit of clays and its engineering implications. *Transp. Res. Rec.* **2009**, *2101*, 34–43. [[CrossRef](#)]
40. Vydehi, K.V.; Moghal, A.A.B.; Basha, B.M. Target Reliability-Based Design of Embankments Using Biopolymer-Modified Cohesive Soil. *Int. J. Geomech.* **2022**, *22*, 04022115. [[CrossRef](#)]

41. Hamza, M.; Nie, Z.; Aziz, M.; Ijaz, N.; Akram, O.; Fang, C.; Madni, M.F. Geotechnical behavior of high-plastic clays treated with biopolymer: Macro–micro-study. *Environ. Earth Sci.* **2023**, *82*, 91. [[CrossRef](#)]
42. Mudgil, D.; Barak, S.; Khatkar, B.S. Guar gum: Processing, properties and food applications—A Review. *J. Food Sci. Technol.* **2014**, *51*, 409–418. [[CrossRef](#)]
43. Fricko, O.; Havlik, P.; Rogelj, J.; Klimont, Z.; Gusti, M.; Johnson, N.; Kolp, P.; Strubegger, M.; Valin, H.; Amann, M.; et al. The marker quantification of the Shared Socioeconomic Pathway 2: A middle-of-the-road scenario for the 21st century. *Glob. Environ. Change* **2017**, *42*, 251–267. [[CrossRef](#)]
44. García-Ochoa, F.; Santos, V.E.; Casas, J.A.; Gómez, E. Xanthan gum: Production, recovery, and properties. *Biotechnol. Adv.* **2000**, *18*, 549–579. [[CrossRef](#)] [[PubMed](#)]
45. Cadmus, M.C.; Rogovin, S.P.; Burton, K.A.; Pittsley, J.E.; Knutson, C.A.; Jeanes, A. Colonial variation in *Xanthomonas campestris* NRRL B-1459 and characterization of the polysaccharide from a variant strain. *Can. J. Microbiol.* **1976**, *22*, 942–948. [[CrossRef](#)] [[PubMed](#)]
46. Palaniraj, A.; Jayaraman, V. Production, recovery and applications of xanthan gum by *Xanthomonas campestris*. *J. Food Eng.* **2011**, *106*, 1–12. [[CrossRef](#)]
47. Vuyst, L.D.; Loo, J.V.; Vandamme, E.J. Two-step fermentation process for improved xanthan production by *Xanthomonas campestris* NRRL-B-1459. *J. Chem. Technol. Biotechnol.* **1987**, *39*, 263–273. [[CrossRef](#)]
48. Souw, P.; Demain, A.L. Nutritional studies on xanthan production by *Xanthomonas campestris* NRRL B1459. *Appl. Environ. Microbiol.* **1979**, *37*, 1186–1192. [[CrossRef](#)]
49. Ascanio, G.; Castro, B.; Galindo, E. Measurement of power consumption in stirred vessels—A review. *Chem. Eng. Res. Des.* **2004**, *82*, 1282–1290. [[CrossRef](#)]
50. Emission Factors for Greenhouse Gas Inventories—U.S. Environmental. 2021. Available online: www.epa.gov/sites/default/files/2021-04/documents/emission-factors_apr2021.pdf (accessed on 4 August 2023).
51. Stafford, F.N.; Raupp-Pereira, F.; Labrincha, J.A.; Hotza, D. Life cycle assessment of the production of cement: A Brazilian case study. *J. Clean. Prod.* **2016**, *137*, 1293–1299. [[CrossRef](#)]
52. Andrew, R.M. Global CO₂ emissions from cement production. *Earth Syst. Sci. Data* **2019**, *10*, 195–217. [[CrossRef](#)]
53. Ashfaq, M.; Lal, M.H.; Moghal, A.A.B.; Murthy, V.R. Carbon Footprint Analysis of Coal Gangue in Geotechnical Engineering Applications. *Indian Geotech. J.* **2020**, *50*, 646–654. [[CrossRef](#)]
54. Ashfaq, M.; Moghal, A.A.B. Cost and carbon footprint analysis of fly ash utilization in Earthworks. *Int. J. Geosynth. Ground Eng.* **2022**, *8*, 21. [[CrossRef](#)]
55. Dowling, A.; O'Dwyer, J.; Adley, C.C. Lime in the limelight. *J. Clean. Prod.* **2015**, *1*, 13–22. [[CrossRef](#)]

Disclaimer/Publisher's Note: The statements, opinions and data contained in all publications are solely those of the individual author(s) and contributor(s) and not of MDPI and/or the editor(s). MDPI and/or the editor(s) disclaim responsibility for any injury to people or property resulting from any ideas, methods, instructions or products referred to in the content.